UV Resonance Raman Investigation of a 3_{10}-Helical Peptide Reveals a Rough Energy Landscape†

Zeeshan Ahmed and Sanford A. Asher*

Department of Chemistry, University of Pittsburgh, Pittsburgh, Pennsylvania 15260

Received May 1, 2006; Revised Manuscript Received May 25, 2006

ABSTRACT: We used UVRRS at 194 and 204 nm excitation to examine the backbone conformation of a 13-residue polypeptide ($gp41_{659-671}$) that has been shown by NMR to predominantly fold into a 3_{10}-helix. Examination of the conformation sensitive $AmIII_3$ region indicates the peptide has significant populations of β-turn, PPII, 3_{10}-helix, and π-helix-like conformations but little α-helix. We estimate that at 1 °C on average six of the 12 peptide bonds are in folded conformations (predominantly 3_{10}- and π-helix), while the other six are in unfolded (β-turn/PPII) conformations. The folded and unfolded populations do not change significantly as the temperature is increased from 1 to 60 °C, suggesting a unique energy landscape where the folded and unfolded conformations are essentially degenerate in energy and exhibit identical temperature dependences.

An understanding of the mechanisms of protein folding will enable the de novo design of proteins with profound commercial and medical applications (*1*−*19*). Over the past 50 years, significant effort to elucidate protein folding and unfolding mechanisms has been expended. Part of this effort has examined the thermodynamics and kinetics of small model systems such as β-hairpins (*20*−*22*) and alanine-based α-helices (*23*−*33*). These studies have provided detailed microscopic knowledge of the folding energy landscape of these isolated motifs. Theoretical simulations have suggested that 3_{10}-helices and/or type III β-turns may serve as intermediates in the α-helix folding pathway (*34*−*39*). The formation of kinetic intermediates such as β-turn or 3_{10}-helix lowers the entropic cost of nucleating the first helical residue, thus facilitating the helix folding transition (*34*, *40*, *41*).

The 3_{10}-helix is the fourth most common secondary structural motif in proteins (*34*−*59*). On average, in proteins, 3−4% of peptide residues occur in a 3_{10}-helix conformation (*48*). The 3_{10}-helix differs from an α-helix in that the tighter packing of the backbone forces the C═O···H−N hydrogen bonds to point outward, away from the helical axis, resulting in decreased stability of the 3_{10}-helix compared to that of the α-helix (*25*, *48*).

Recent ESR (*39*, *42*) and NMR (*43*) work by Millhauser et al. (*41*) suggests the presence of 3_{10}-helix at the terminus of short alanine-based helical peptides. The authors proposed that 3_{10}-helices are a relic of the folding process. They reasoned that nascent helices contain mixtures of unfolded and turn conformations, specifically type III turns. As folding conditions begin to favor helical structures, the type III turn conformation (a single 3_{10}-helix unit) propagates; i.e., the chain adopts a 3_{10}-helix conformation. As the helical domain lengthens, the α-helix conformation competes with the 3_{10}-helix conformation. Finally, at longer helical lengths, the α-helix conformation dominates. Some 3_{10}-helix/type III turn-like conformations may survive at the termini (*41*).

It should be noted that Millhauser's results have been disputed by Smythe et al. (*44*), who argued that the rotational diffusion of the flexible labels used in the ESR study of Milhauser et al. (*41*) confounded spectral interpretation. Using Toac residues as ESR labels, Smythe et al. found no evidence for a significant 3_{10}-helix population in a 17-residue, alanine-based helical peptide (*44*).

The inability to characterize simple monomeric 3_{10}-helices is a major stumbling block in advancing our understanding of the α-helix (un)folding process; furthermore, the lack of such a model system has made unambiguous identification of 3_{10}-helix spectroscopic markers difficult. Schievano et al. (*45*) recently reported the first water soluble 3_{10}-helix; however, this particular peptide consisted of unnatural amino acids. Unfortunately, the conformation dynamics of peptides with unnatural amino acids may be irrelevant for the study of biological problems. In this context, the recent discovery of Biron et al. of an all-natural amino acid tridecapeptide, $gp41_{659-671}$ (*48*), that folds into a 3_{10}-helix is greatly significant since it enables the study of 3_{10}-helices.

$gp41_{659-671}$ is a 13-residue peptide with the sequence E_{659}-LLELDKWAS_{669}LWN extracted from glycoprotein gp41 of HIV-1, corresponding to residues 659−671. NOE constraints indicate that in water at 277 K, the monomeric form of the peptide folds into a nine-residue 3_{10}-helix (*48*). Biron et al. proposed that the 3_{10}-helix is stabilized by favorable hydrophobic stacking interactions between L663, W666, L669, and W670 (*48*). Residues E662, K665, S668, and N671 form the polar face where E662 and K665 may engage in weak electrostatic interactions. Burial of considerable hydrophobic surface area is proposed to favor the 3_{10}-helix over the α-helix conformation (*48*).

In this work, we used UV[1] resonance Raman spectroscopy to examine $gp41_{659-671}$'s conformation. We studied the

† This work was supported by NIH Grant 8 RO1 EB002053021.

* To whom correspondence should be addressed. Phone: (412) 624-8570. Fax: (412) 624-0588. E-mail: asher@pitt.edu.

10.1021/bi060858m CCC: $33.50
Published on Web 07/06/2006

peptide secondary structure by exciting within the amide $\pi \rightarrow \pi^*$ transition with 204 and 194 nm excitation. Our results indicate that the 3_{10}-helix is in equilibrium with multiple secondary structures, namely, the π-helix, β-turns, and PPII conformation, creating an energy landscape where the folded and unfolded conformations are essentially degenerate in energy and exhibit identical temperature dependences.

EXPERIMENTAL PROCEDURES

The UV resonance Raman spectrometer has been described in detail elsewhere (*60*). Briefly, 204 nm UV light was generated by generation of the fifth anti-Stokes Raman harmonic of the third harmonic of a Nd:YAG laser (Coherent, Infinity). The 194 nm deep UV light was generated as the ($3\omega + \omega$) fourth harmonic of a diode-pumped Ti:sapphire laser (Positive Light, Indigo-S). The sample was circulated in a free surface, temperature-controlled stream. A 135° backscattering geometry was used for sampling. The collected light was dispersed by a subtractive double monochromator onto a back-thinned CCD camera (Princeton Instruments, Spec 10).

The $gp41_{659-671}$ peptide was obtained from the Pittsburgh Peptide Synthesis Facility (>95% pure) and used at a concentration of 1 mg/mL at pH 7. UVRR spectra measured at 20 °C during and after the Raman measurements were essentially identical, indicating the lack of significant photo degradation and/or thermal degradation. Raman spectra were normalized relative to the peak height of the 932 cm^{-1} ClO_4^- band. Concentrations of ClO_4^- of 0.05 and 0.1 M were used for the 204 and 194 nm excited UVRR measurements. Helix promoter TFE was acquired form Aldrich. The solution pH was adjusted by adding small aliquots of dilute HCl or NaOH. CD measurements were carried out on a JASCO 710 spectrometer using a peptide concentration of 0.3 mg/mL.

RESULTS AND DISCUSSION

Excitation (204 nm) Temperature Dependence. The 204 nm excitation Raman spectra (Figure 1) show bands arising from amide and to a lesser extent Trp vibrations. To facilitate spectral interpretation, we subtracted the Trp contribution from the temperature-dependent 204 nm excited $gp41_{659-671}$ spectra (Figure 2). The band intensities of the resulting spectra were normalized with respect to the AmI band intensity. The spectra show an AmI vibration at 1668 cm^{-1} which is predominantly a C═O stretching vibration (*61*, *62*). The 1556 cm^{-1} molecular oxygen stretching band (*32*, *63*) overlaps with the 1558 cm^{-1} AmII band. The AmII vibration involves C−N stretching with some N−H bending (*61*, *62*). The trough in the 1420−1500 cm^{-1} region is due to the 1483 cm^{-1} COO^- stretching band from the Trp monomer which was subtracted from the original peptide spectra (*64*, *65*).

A weak 1355 cm^{-1} band ($AmIII_1$/residual W7) appears as a shoulder on the 1390 cm^{-1} C_α−H bending band. The C_α−H bending band intensity is derived from non-α-helical peptide bond conformations (*61*, *66*). A weak $AmIII_2$ band is located at ∼1320 cm^{-1}. A broad $AmIII_3$ band [predominantly C−N stretching and N−H bending mode (*61*, *66*−*69*)] at 1257 cm^{-1} shows additional features at 1293 and 1226 cm^{-1}. Mikhonin et al. (*70*) recently demonstrated that the "pure" α-helix UVRR spectra show a narrow $AmIII_3$ band centered at 1260 cm^{-1} (Figure 2). The presence of a broad $AmIII_3$ band here indicates the existence of multiple conformations in $gp41_{659-671}$.

As the solution temperature is increased from 1 to 30 °C, the 1390 cm^{-1} C_α−H_b and $AmIII_3$ bands show a slight decrease in intensity (Figure 2). A similar temperature-induced intensity decrease was previously observed for a water-exposed, PPII peptide whose conformation was temperature-independent (*24*, *67*). The lack of conformation-induced changes in the $AmIII_3$ and C_α−H_b region suggests that $gp41_{659-671}$ does not undergo a thermally induced helix melting transition between 1 and 30 °C.

We can quantitate the number of helical amide bonds by using the Raman cross section of the C_α−H bending band

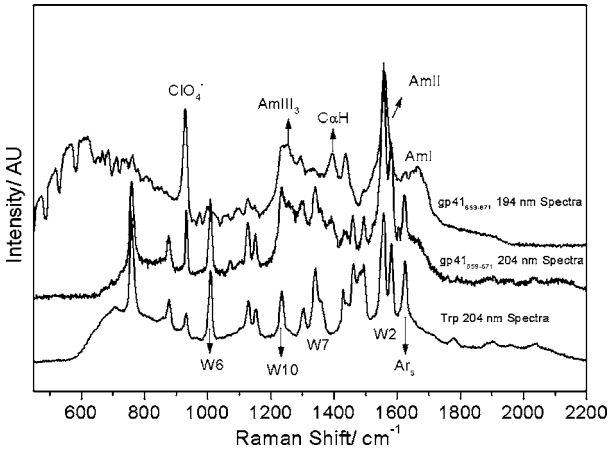

FIGURE 1: UV resonance Raman spectra (204 and 194 nm) of $gp41_{659-671}$ measured at 1 °C. Also displayed are the 204 nm excitation UVRR spectra of the Trp monomer, where the 1483 cm^{-1} carboxylate stretching band overlaps with the W4 and W5 bands of Trp. As compared to the 204 nm spectra, the 194 nm excited $gp41_{659-671}$ spectra show considerably less Trp spectral contribution. The smaller Trp contribution allows us to resolve amide bands from overlapping Trp bands.

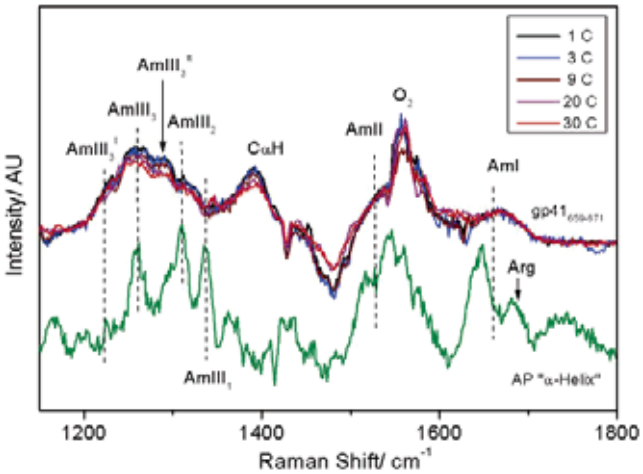

FIGURE 2: Top traces are 204 nm UV resonance Raman spectra of $gp41_{659-671}$ measured between 1 and 30 °C. To facilitate spectral interpretation, the Trp contribution was subtracted. The resulting spectra exhibit resonance-enhanced amide vibrations. Below, the green trace shows the 204 nm excited pure α-helix spectra of AP peptide (adapted from ref *70*) which shows its characteristic narrow $AmIII_3$ band at 1260 cm^{-1}.

[1] Abbreviations: UV, ultraviolet; UVRRS, resonance Raman spectroscopy; CD, circular dichroism; Am, amide; NOE, nuclear Overhauser effect; TFE, 2,2,2-trifluoroethanol.

from a 21-residue, alanine-based, mostly α-helical peptide known as AP (*24*); we are utilizing the assumption that the $gp41_{659-671}$'s unfolded segment $C_\alpha-H$ bending bands have Raman cross sections similar to those of the unfolded/PPII conformation of AP. This is a reasonable estimate since $C_\alpha-H_b$ bands have similar cross sections in the PPII and extended *β*-strand conformations (*61*); we expect similar coupling between $C_\alpha-H_b$ and $N-H_b$ bands for peptide bonds with similar Ψ angles (*69*). Since the α-helix and the 3_{10}-helix conformations have similar Ψ angles (*45*), we assume that as in the α-helix, the putative 3_{10}-helix will exhibit a negligible $C_\alpha-H$ band intensity. Thus, we use the $C_\alpha-H$ band intensity to estimate the number of bonds in the PPII conformation. On the basis of the $C_\alpha-H$ band cross sections of the alanine-based, mainly α-helical peptide AP (see ref *19*), we calculate the number of nonhelical amide bonds in $gp41_{659-671}$ as

$$n_A = (I_{C\alpha H}N_{ClO_4} - \sigma_{ClO_4^-})/(\sigma_{C\alpha H}N_P I_{ClO_4^-}) \quad (1)$$

where $\sigma_{C\alpha H}$ and $\sigma_{ClO_4^-}$ are the Raman cross sections of the $C_\alpha-H$ band and the 932 cm^{-1} perchlorate band, respectively. $N_{ClO_4^-}$ and N_P are the numbers of perchlorate and $gp41_{659-671}$ molecules in the scattering volume, respectively. $I_{ClO_4^-}$ is the perchlorate band (932 cm^{-1}) intensity, while $I_{C\alpha H}$ is the intensity of the $C_\alpha-H$ band. n_A is the number of amide peptide bonds in $gp41_{659-671}$ which contribute to intensity $I_{C\alpha H}$. We calculate that at 1 °C six of 12 peptide bonds are in a PPII-like conformation while six peptide bonds adopt α-helix-like conformations.

As noted above, $gp41_{659-671}$ does not exhibit a temperature-dependent decrease in helicity. The observed behavior can be rationalized by requiring the folded and unfolded state ensembles to be nearly degenerate in energy and equally disordered; i.e., the number of conformations comprising the folded and unfolded state are nearly equal. Under such circumstances, the peptide has an equal probability of populating either a helix or unfolded state, and as such, their relative population distribution would not be impacted by an increase in temperature. These results are consistent with the study of Biron et al., who reported a lack of 3_{10}-helix melting with an increase in temperature (*48*).

The $gp41_{659-671}$ peptide, however, does exhibit a conformation change in TFE/water solutions (Figure 3). Manning and Woody (*71*) proposed that the CD spectra of 3_{10}- and α-helix should show different values of *R* ($\Theta_{222}/\Theta_{207}$). The 3_{10}-helix is expected to exhibit a lower *R* value (~0.3) than the α-helix (~1). Additionally, the 3_{10}-helix is expected to exhibit a weak positive band at ~195 nm, while the α-helix shows a relatively strong positive band at ~195 nm (*59*, *71*). As shown in Figure 3 (inset), the CD spectra show an *R* value of ~0.3 in water and water/TFE solutions indicating the presence of 3_{10}-helices. In water, we observe a negative maximum at 200 nm without a trough at 222 nm. This suggests a significant population of unfolded conformations; UVRR indicates only 50% helicity in water. Our CD spectra of $gp41_{659-671}$ differ from those of Biron et al. in that their peptide spectra in pure water exhibit greater 3_{10}-helix content. We do not know the reason for differences in the two measurements. Addition of 10% TFE does not impact the position of the 200 nm negative band, but 30% TFE red shifts the band maxima to 205 nm, indicating increased 3_{10}-helix content. These results are confirmed by our UVRR measurements where the peptide spectra in 10% TFE exhibit ~55% helicity, whereas in 30% TFE, the peptide exhibits negligible $C_\alpha-H$ band intensity, indicating ~92% helicity (Figure 3). The TFE-stabilized helix does not exhibit any appreciable melting with an increase in temperature (not shown).

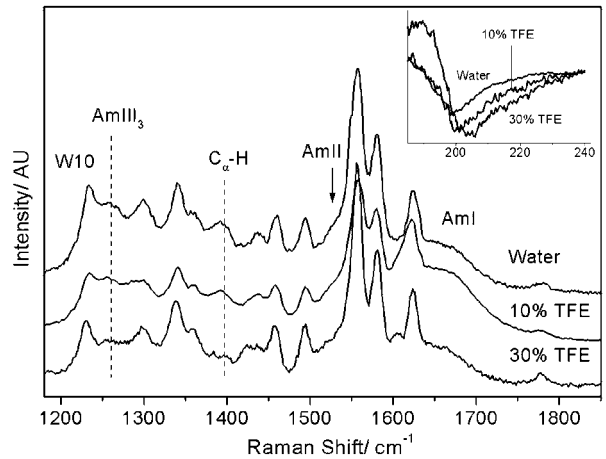

FIGURE 3: UV resonance Raman spectra (204 nm) of $gp41_{659-671}$ in pure water or 10 or 30% (v/v) TFE at 1 °C. The TFE contribution has been subtracted from the spectra. The resulting spectra show bands arising from amide and Trp vibrations. In 10% TFE, the presence of a $C_\alpha-H$ band indicates ~55% helicity, whereas in 30% TFE, the $C_\alpha-H$ band shows negligible band intensity, indicating a 92% helical content. The inset shows CD spectra of $gp41_{659-671}$ in water and 10 and 30% (v/v) TFE solutions. As discussed in the text, these CD spectra show the peptide's 3_{10}-helix content increases with TFE concentration.

It should be noted that our UVRR results do not necessarily suggest that a single, continuous 3_{10}-helix of six peptide bonds exists in water. Recently, Mikhonin and Asher (*72*) demonstrated that the resonance-enhanced AmIII and $C_\alpha-H$ bands scatter independently; i.e., there is negligible coupling between adjacent peptide bonds. Hence, the UVRR spectra in the AmIII and $C_\alpha-H$ region can be regarded as a linear sum of individual peptide bonds. We therefore envision a scenario in which, in water, the peptide is flickering between folded and unfolded conformations; the observed $C_\alpha-H$ band intensity is, therefore, a measure of the peptide's residence time in extended PPII-like conformations. Hence, the observed 50% helical content could indicate that during the measurement period a peptide bond has an equal probability of being in the folded or unfolded/extended conformation regions of the Ramachandran space.

CONFORMATION ANALYSIS

The conformational space sampled by the $gp41_{659-671}$ peptide in water can be quantitatively analyzed by an examination of the $AmIII_3$ region. The subtraction of the Trp contribution, however, results in a noisy spectrum which complicates assignment of the $AmIII_3$ bands. Previously, Fodor et al. (*73*) reported that Trp cross sections weaken at shorter excitation wavelengths. Thus, by exciting the samples at 194 nm, we are able to selectively enhance the amide vibrations relative to Trp vibrations and acquire spectra dominated by amide vibrations.

We deconvoluted the measured 194 nm excitation spectrum into a sum of a minimum number of Voight bands by using the peak fitting routine in Grams version 5 (Galactic

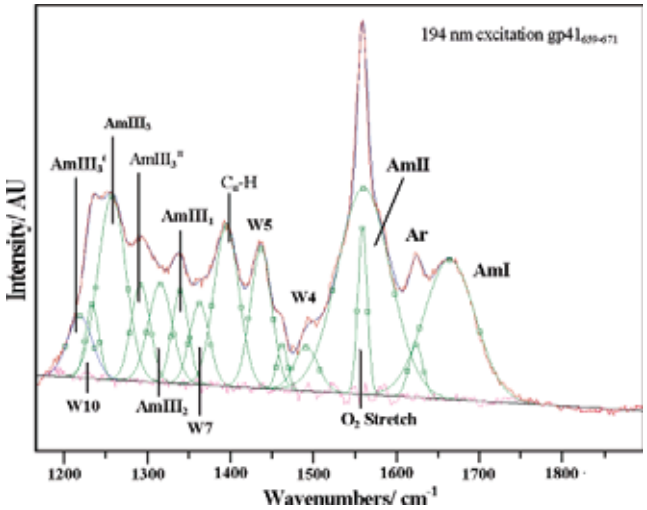

FIGURE 4: Spectral deconvolution of 1 °C, 194 nm UVRR $gp41_{659-671}$ spectra with Voight bands. The excellence of the fit is evident from the flat residual displayed underneath.

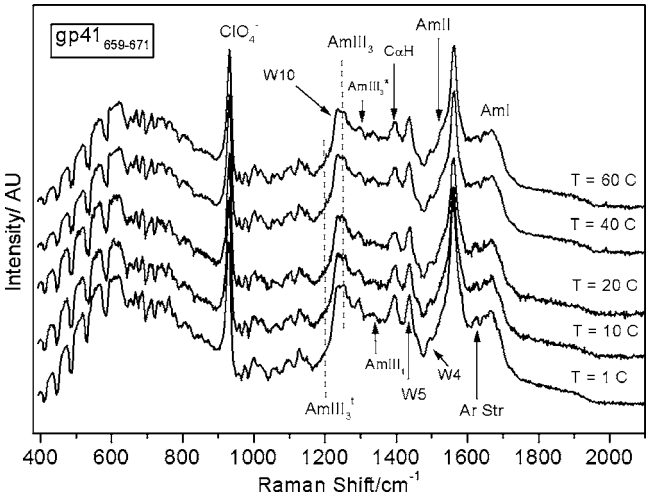

FIGURE 5: UV resonance Raman spectra (194 nm) of $gp41_{659-671}$ measured between 1 and 60 °C. Three 10 min spectra were summed and scaled to the intensity of the 932 cm^{-1} perchlorate band. The bands arise mainly from amide vibrations except for those that derive from Trp ring vibrations.

Industries Corp., Figure 4). The 194 nm excitation UVRR spectra show an AmI band at 1664 cm^{-1} with a weak aromatic stretching band at 1665 cm^{-1}. The decreased aromatic stretching band intensity allows us to resolve the AmI band. An increased contribution from diatomic oxygen interferes with the AmII band located at ~1556 cm^{-1}. The W4 and W5 Trp bands are located at 1491 and 1437 cm^{-1}. An intense C_α−H bending band located at 1394 cm^{-1} shows an only negligible temperature-induced decrease in intensity (Figure 5). A small $AmIII_1$ band at 1340 cm^{-1} overlaps the W7 band of Trp, while a weak $AmIII_2$ band is observed at ~1300 cm^{-1}. As with 204 nm excitation, we observe $AmIII_3$ bands at 1293, 1254, and 1224 cm^{-1}. As the temperature is increased from 1 to 60 °C, the AmII band intensity decreases while the band position downshifts from 1560 to 1557 cm^{-1} (Figure 5). The $AmIII_1$, $AmIII_2$, and 1293 cm^{-1} $AmIII_3$ band position remain more or less invariant with an increase in temperature. The broad 1254 cm^{-1} $AmIII_3$ band downshifts, while the 1224 cm^{-1} $AmIII_3$ band exhibits an increased band intensity with an increase in temperature.

Recently, Mikhonin et al. (*74*) quantitatively demonstrated that the $AmIII_3$ band frequency depends on the ψ dihedral angle and the hydrogen bonding state of amide bond ψ (*67*, *74*). Using their methodology for correlating the ψ dihedral angle with the $AmIII_3$ band position, we determine that the 1224 cm^{-1} band could originate from either the distorted β-sheet ($\psi = 40°$) or β-turn-like ($\psi = -3°$) conformations.

In the 277−302 K temperature interval, Biron et al. (*48*) using analytical ultracentrifugation did not observe any significant aggregation or dimerization products of $gp41_{659-671}$. We therefore conclude that the 1224 cm^{-1} band originates from β-turn conformations and assign the 1224 cm^{-1} band as the β-turn amide III_3 ($AmIII_3^t$). The ψ dihedral angle of −3° indicated by the $AmIII_3^t$ band position suggests the presence of type I turns.

The 1293 cm^{-1} $AmIII_3$ band does not exhibit any significant temperature-dependent shift in band position, indicating a conformation dominated by intrapeptide hydrogen bonds. According to the data of Mikhonin et al. (*74*), the band position likely correlates to a ψ of −75°, suggesting the presence of a π-helix-like conformation. Previous studies of peptides with significant 3_{10}-helix populations found appreciable π-helix populations in equilibrium with the native helix (*38*, *46*). MD simulations suggest that the π-helix may serve as an intermediate in the α-helix folding pathway (*38*). Alternatively, Cartailler and Luecke suggest π-helices exist as defects in α-helices where the presence of a π-helix-like 1 → 5 hydrogen bond (π-bulge) introduces a kink into the α-helix (*75*).

The broad 1254 cm^{-1} $AmIII_3$ band is composed of overlapping helical and PPII conformations. The 1254 cm^{-1} band maximum indicates a dominant 3_{10}-helix conformation, though it should be noted that the type III turn conformation (a single 3_{10}-helix unit) is expected to contribute in this frequency region as it populates similar dihedral angles (*41*). Typical α-helical peptides show an $AmIII_3$ band maximum at 1263 cm^{-1}. The 9 cm^{-1} shift in the $AmIII_3$ band position of $gp41_{659-671}$ as compared to typical α-helical peptides such as the AP peptide (*24*) indicates the average ψ angle of $gp41_{659-671}$ deviates from the typical α-helix conformation by 10°. This result demonstrates that UVRR can discriminate between conformationally similar α- and 3_{10}-helicies.

Recent MD simulations have suggested that distorted α-helices exist in a rapid equilibrium with the 3_{10}-helix conformations (*76*). While we do not find any definitive evidence of significant concentration of α-helix conformation, the broad width of the $AmIII_3$ band suggests that a small α-helix population may exist (see Figure 2).

CONCLUSIONS

We examined the secondary structure of $gp41_{659-671}$ by exciting the backbone at 204 and 194 nm. Our results indicate that six of the 12 peptide bonds adopt helical conformations (predominantly 3_{10}- or π-helix). An examination of the conformation sensitive $AmIII_3$ region indicates $gp41_{659-671}$ exhibits a broad distribution of conformations that includes PPII, β-turn, 3_{10}-helix, and π-helix conformations but little α-helix; furthermore, we demonstrate that the $AmIII_3$ band position can be used to distinguish a 3_{10}-helix from an α-helix conformation. A lack of temperature-induced change in the $AmIII_3$ band intensities indicates an energy landscape where

the helical and unfolded conformations occupy degenerate energy levels with similar entropies. This allows for nearly equal populations of both the helical and unfolded conformations, as evidenced by the C_α−H band intensity which indicates a 50% helical content, independent of temperature.

ACKNOWLEDGMENT

We thank Prof. J. Anglister, Prof. C. Toniolo, Prof. A. Ozdemir, A. V. Mikhonin, and Dr. N. Myshakina for helpful discussions and Prof. C. Schafmeister for donating the TFE sample.

REFERENCES

1. Anfinsen, C. B. (1973) Principles that govern the folding of protein chains, *Science 181*, 223−30.
2. Chan, H. S., and Dill, K. A. (1998) Protein folding in the landscape perspective: Chevron plots and non-Arrhenius kinetics, *Proteins: Struct., Funct., Genet. 30*, 2−33.
3. Dill, K. A. (1990) Dominant Forces in Protein Folding, *Biochemistry 29*, 7133−55.
4. Jewett, A. I., Pande, V. S., and Plaxco, K. W. (2003) Cooperativity, Smooth Energy Landscapes and the Origins of Topology-dependent Protein Folding Rates, *J. Mol. Biol. 326*, 247−53.
5. Hardin, C., Eastwood, M. P., Prentiss, M., Luthey-Schulten, Z., and Wolynes, P. G. (2002) Folding funnels: The key to robust protein structure prediction, *J. Comput. Chem. 23*, 138−46.
6. Cleland, J. (1993) *Protein Folding: In Vivo and In Vitro*, American Chemical Society, Washington, DC.
7. Dill, K. A., Alonso, D. O. V., and Hutchinson, K. (1989) Thermal stabilities of globular proteins, *Biochemistry 28*, 5439−49.
8. Glaser, R. (2000) *Biophysics*, Springer, New York.
9. Alm, E., and Baker, D. (1999) Prediction of protein-folding mechanisms from free-energy landscapes derived from native structures, *Proc. Natl. Acad. Sci. U.S.A. 96*, 11305−10.
10. Wolynes, P. G., Onuchic, J. N., and Thirumalai, D. (1995) Navigating the folding routes, *Science 267*, 1619−20.
11. Pappu, R. V., Srinivasan, R., and Rose, G. D. (2000) The Flory isolated-pair hypothesis is not valid for polypeptide chains: Implications for protein folding, *Proc. Natl. Acad. Sci. U.S.A. 97*, 12565−70.
12. Myers, J. K., and Oas, T. G. (2002) Mechanisms of fast protein folding, *Annu. Rev. Biochem. 71*, 783−815.
13. Shortle, D. (1993) Denatured states of proteins and their roles in folding and stability, *Curr. Opin. Struct. Biol. 3*, 66−74.
14. Bryngelson, J. D., and Wolynes, P. G. (1989) Intermediates and barrier crossing in a random energy model (with applications to protein folding), *J. Phys. Chem. 93*, 6902−15.
15. Hao, M.-H., and Scheraga Harold, A. (1994) Statistical thermodynamics of protein folding: Sequence dependence, *J. Phys. Chem. 98*, 9882−93.
16. Dobson, C. M., Salij, A., and Karplus, M. (1998) Protein Folding: A Perspective from Theory and Experiment, *Angew. Chem., Int. Ed. 37*, 868−93.
17. Munoz, V., Thompson, P. A., Hofrichter, J., and Eaton, W. A. (1997) Folding dynamics and mechanism of β-hairpin formation, *Nature 390*, 196−9.
18. Urry, D. W. (1997) Physical Chemistry of Biological Free Energy Transduction As Demonstrated by Elastic Protein-Based Polymers, *J. Phys. Chem. B 101*, 11007−28.
19. Ahmed, Z., Illir, A. B., Mikhonin, A. V., and Asher, S. A. (2005) UV-Resonance Raman Thermal Unfolding Study of Trp-Cage Shows That It Is Not a Simple Two-State Miniprotein, *J. Am. Chem. Soc. 127*, 10943−50.
20. Eaton, W. A., Munoz, V., Thompson, P. A., Henry, E. R., and Hofrichter, J. (1998) Kinetics and Dynamics of Loops, α-Helices, β-Hairpins, and Fast-Folding Proteins, *Acc. Chem. Res. 31*, 745−53.
21. Munoz, V., Henry, E. R., Hofrichter, J., and Eaton, W. A. (1998) A statistical mechanical model for β-hairpin kinetics, *Proc. Natl. Acad. Sci. U.S.A. 95*, 5872−9.
22. Dinner, A. R., Lazaridis, T., and Karplus, M. (1999) Understanding β-hairpin formation, *Proc. Natl. Acad. Sci. U.S.A. 96*, 9068−73.
23. Thompson, P. A., Eaton, W. A., and Hofrichter, J. (1997) Laser Temperature Jump Study of the Helix-Coil Kinetics of an Alanine Peptide Interpreted with a 'Kinetic Zipper' Model, *Biochemistry 36*, 9200−10.
24. Lednev, I. K., Karnoup, A. S., Sparrow, M. C., and Asher, S. A. (1999) α-Helix peptide folding and unfolding activation barriers: A nanosecond UV resonance Raman study, *J. Am. Chem. Soc. 121*, 8074−86.
25. Bolin, K. A., Pitkeathly, M., Miranker, A., Smith, L. J., and Dobson, C. M. (1996) Insight into a random coil conformation and an isolated helix: Structural and dynamical characterisation of the C-helix peptide from hen lysozyme, *J. Mol. Biol. 261*, 443−53.
26. Garcia, A. E., and Sanbonmatsu, K. Y. (2002) α-Helical stabilization by side chain shielding of backbone hydrogen bonds, *Proc. Natl. Acad. Sci. U.S.A. 99*, 2782−7.
27. Andrew, C. D., Warwicker, J., Jones, G. R., and Doig, A. J. (2002) Effect of Phosphorylation on α-Helix Stability as a Function of Position, *Biochemistry 41*, 1897−905.
28. Lednev, I. K., Karnoup, A. S., Sparrow, M. C., and Asher, S. A. (2001) Transient UV Raman spectroscopy finds no crossing barrier between the peptide α-helix and fully random coil conformation, *J. Am. Chem. Soc. 123*, 2388−92.
29. Woutersen, S., and Hamm, P. (2001) Isotope-Edited Two-Dimensional Vibrational Spectroscopy of Trialanine in Aqueous Solution, *J. Chem. Phys. 114*, 2727−37.
30. Clarke, D. T., Doig, A. J., Stapley, B. J., and Jones, G. R. (1999) The α-helix folds on the millisecond time scale, *Proc. Natl. Acad. Sci. U.S.A. 96*, 7232−7.
31. Williams, S., Causgrove, T. P., Gilmanshin, R., Fang, K. S., Callender, R. H., Woodruff, W. H., and Dyer, R. B. (1996) Fast Events in Protein Folding: Helix Melting and Formation in a Small Peptide, *Biochemistry 35*, 691−7.
32. Ianoul, A., Mikhonin, A., Lednev, I. K., and Asher, S. A. (2002) UV Resonance Raman Study of the Spatial Dependence of α-Helix Unfolding, *J. Phys. Chem. A 106*, 3621−4.
33. Asher, S. A., Mikhonin, A. V., and Bykov, S. V. (2004) UV Raman Demonstrates that α-Helical Polyalanine Peptides Melt to Polyproline II Conformations, *J. Am. Chem. Soc. 126*, 8433−40.
34. Sheinerman, F. B., and Brooks Charles, L., III (1995) 3_{10} Helixes in Peptides and Proteins As Studied by Modified Zimm-Bragg Theory, *J. Am. Chem. Soc. 117*, 10098−103.
35. Sung, S.-S. (1995) Folding simulations of alanine-based peptides with lysine residues, *Biophys. J. 68*, 826−34.
36. Tobias, D. J., and Brooks Charles, L., III (1991) Thermodynamics and mechanism of α-helix initiation in alanine and valine peptides, *Biochemistry 30*, 6059−70.
37. Young, W. S., and Brooks Charles, L., III (1995) Molecular Dynamics Simulations of Isolated Helixes of Myoglobin, *Biochemistry 34*, 7614−21.
38. Armen, R., Alonso, D. O. V., and Daggett, V. (2003) The role of α-, 3_{10}-, and π-helix in helix-coil transitions, *Protein Sci. 12*, 1145−57.
39. Fiori, W. R., Miick, S. M., and Millhauser, G. L. (1993) Increasing sequence length favors α-helix over 3_{10}-helix in alanine-based peptides: Evidence for a length-dependent structural transition, *Biochemistry 32*, 11957−62.
40. Sundaralingam, M., and Sekharudu, Y. C. (1989) Water-inserted α-helicies segments implicate reverse turns as folding intermediates, *Science 244*, 1333−7.
41. Millhauser, G. L. (1995) Views of Helical Peptides: A Proposal for the Position of 3_{10}-Helix along the Thermodynamic Folding Pathway, *Biochemistry 34*, 3873−7.
42. Miick, S. M., Martinez, G. V., Fiori, W. R., Todd, A. P., and Millhauser, G. L. (1992) Short alanine-based peptides may form 3_{10}-helices and not α-helices in aqueous solution, *Nature 359*, 653−5.
43. Millhauser, G. L., Stenland, C. J., Hanson, P., Bolin, K. A., and van de Ven, F. J. M. (1997) Estimating the relative populations of 3_{10}-helix and α-helix in Ala-rich peptides: A hydrogen exchange and high field NMR study, *J. Mol. Biol. 267*, 963−74.
44. Smythe, M. L., Huston, S. E., and Marshall, G. R. (1995) The Molten Helix: Effects of Solvation on the α- to 3_{10}-Helical Transition, *J. Am. Chem. Soc. 117*, 5445−52.
45. Schievano, E., Bisello, A., Chorev, M., Bisol, A., Mammi, S., and Peggion, E. (2001) Aib-Rich Peptides Containing Lactam-Bridged Side Chains as Models of the 3_{10}-Helix, *J. Am. Chem. Soc. 123*, 2743−51.
46. Kim, S. W., and Cross, T. A. (2004) 2D solid-state NMR spectral simulation of 3_{10}, α, and π-helices, *J. Magn. Reson. 168*, 187−366.

47. Toniolo, C., Formaggio, F., Tognon, S., Broxterman, Q. B., Kaptein, B., Huang, R., Setnicka, V., Keiderling, T. A., McColl, I. H., Hecht, L., and Barron, L. D. (2004) The complete chirospectroscopic signature of the peptide 3_{10}-helix in aqueous solution, *Biopolymers 75*, 32−45.
48. Biron, Z., Khare, S., Samson, A. O., Hayek, Y., Naider, F., and Anglister, J. (2002) A Monomeric 3_{10}-Helix Is Formed in Water by a 13-Residue Peptide Representing the Neutralizing Determinant of HIV-1 on gp41, *Biochemistry 41*, 12687−96.
49. Andersen, N. H., Liu, Z., and Prickett, K. S. (1996) Efforts toward deriving the CD spectrum of a 3_{10} helix in aqueous medium, *FEBS Lett. 399*, 47−52.
50. Hanson, P., Anderson, D. J., Martinez, G., Millhauser, G. L., Formaggio, F., Crisma, M., Toniolo, C., and Vita, C. (1998) Electron spin resonance and structural analysis of water soluble, alanine-rich peptides incorporating TOAC, *Mol. Phys. 95*, 957−66.
51. Basu, G., Kitao, A., Hirata, F., and Go, N. (1994) A Collective Motion Description of the 3_{10}-/α-Helix Transition: Implications for a Natural Reaction Coordinate, *J. Am. Chem. Soc. 116*, 6307−15.
52. Gratias, R., Konat, R., Kessler, H., Crisma, M., Valle, G., Polese, A., Formaggio, F., Toniolo, C., Broxterman, Q. B., and Kamphuis, J. (1998) First Step Toward the Quantitative Identification of Peptide 3_{10}-Helix Conformation with NMR Spectroscopy: NMR and X-ray Diffraction Structural Analysis of a Fully-Developed 310-Helical Peptide Standard, *J. Am. Chem. Soc. 120*, 4763−70.
53. Yasui, S. C., Keiderling, T. A., Formaggio, F., Bonora, G. M., and Toniolo, C. (1986) Vibrational circular dichroism of polypeptides. 9. A study of chain length dependence for 3_{10}-helix formation in solution, *J. Am. Chem. Soc. 108*, 4988−93.
54. Wieczorek, R., and Dannenberg, J. J. (2003) Hydrogen-Bond Cooperativity, Vibrational Coupling, and Dependence of Helix Stability on Changes in Amino Acid Sequence in Small 3_{10}-Helical Peptides. A Density Functional Theory Study, *J. Am. Chem. Soc. 125*, 14065−71.
55. Kennedy, D. F., Crisma, M., Toniolo, C., and Chapman, D. (1991) Studies of peptides forming 3_{10}- and α-helixes and β-bend ribbon structures in organic solution and in model biomembranes by Fourier transform infrared spectroscopy, *Biochemistry 30*, 6541−8.
56. Zhang, L., and Hermans, J. (1994) 310 Helix Versus α-Helix: A Molecular Dynamics Study of Conformational Preferences of Aib and Alanine, *J. Am. Chem. Soc. 116*, 11915−21.
57. Kubelka, J., Silva, G. D., and Keiderling, T. A. (2002) Discrimination between Peptide 3_{10}- and α-Helices. Theoretical Analysis of the Impact of α-Methyl Substitution on Experimental Spectra, *J. Am. Chem. Soc. 124*, 5325−32.
58. Toniolo, C., Bonora, G. M., Bavoso, A., Benedetti, E., Di Blasio, B., Pavone, V., and Pedone, C. (1986) A long, regular polypeptide 3_{10}-helix, *Macromolecules 19*, 472−9.
59. Toniolo, C., Polese, A., Formaggio, F., Crisma, M., and Kamphuis, J. (1996) Circular Dichroism Spectrum of a Peptide 3_{10}-Helix, *J. Am. Chem. Soc. 118*, 2744−5.
60. Bykov, S. B., Lednev, I. K., Ianoul, A., Mikhonin, A. V., and Asher, S. A. (2005) Steady State and Transient UV Resonance Raman Spectrometer for the 193−270 nm Spectral Region, *Appl. Spectrosc. 59*, 1541−52.
61. Chi, Z., Chen, X. G., Holtz, J. S. W., and Asher, S. A. (1998) UV Resonance Raman-Selective Amide Vibrational Enhancement: Quantitative Methodology for Determining Protein Secondary Structure, *Biochemistry 37*, 2854−64.
62. Mirkin, N. G., and Krimm, S. (1996) Ab initio vibrational analysis of isotopic derivatives of aqueous hydrogen-bonded trans-*N*-methylacetamide, *J. Mol. Struct. 377*, 219−34.
63. Matsui, T., Chenung, A. S.-C., Leung, K. W.-S., Yoshino, K., Parkinson, W. H., Thorne, A. P., Murray, J. E., Ito, K., and Imajo, T. (2003) High-resolution absorption cross-section measurements of the Schumann−Runge bands of O_2 by VUV Fourier transform spectroscopy, *J. Mol. Spectrosc. 219*, 45−57.
64. Pajcini, V., Chen, X. G., Bormett, R. W., Geib, S. J., Li, P., Asher, S. A., and Lidiak, E. G. (1996) Glycylglycine p → p and Charge-Transfer Transition Moment Orientations: Near-Resonance Raman Single-Crystal Measurement, *J. Am. Chem. Soc. 118*, 9705−15.
65. Chen, X. G., Li, P., Holtz, J. S. W., Chi, Z., Pajcini, V., Asher, S. A., and Kelly, L. A. (1996) Resonance Raman Examination of the Electronic Excited States of Glycylglycine and Other Dipeptides: Observation of a Carboxylate → Amide Charge Transfer Transition, *J. Am. Chem. Soc. 118*, 9716−26.
66. Wang, Y., Purrello, R., Jordan, T., and Spiro, T. G. (1991) UVRR spectroscopy of the peptide bond. 1. Amide S, a nonhelical structure marker, is a CaH bending mode, *J. Am. Chem. Soc. 113*, 6359−68.
67. Mikhonin, A. V., Ahmed, Z., Ianoul, A., and Asher, S. A. (2004) Assignment and Conformational Dependencies of the Amide III Peptide Backbone UV Resonance Raman bands, *J. Phys. Chem. B 108*, 19020−8.
68. Mikhonin, A. V., Myshakina, N. S., Bykov, S. V., and Asher, S. A. (2005) UV Resonance Raman Spectroscopic Detection of Polyproline II, Extended 5/1-Helix and β-Sheet Conformations of Poly-L-Lysine and Poly-L-Glutamic Acid, *J. Am. Chem. Soc. 127*, 7712−20.
69. Asher, S. A., Ianoul, A., Mix, G., Boyden, M. N., Karnoup, A., Diem, M., and Schweitzer-Stenner, R. (2001) Dihedral ψ angle dependence of the amide III vibration: A uniquely sensitive UV resonance Raman secondary structural probe, *J. Am. Chem. Soc. 123*, 11775−81.
70. Mikhonin, A. V., and Asher, S. A. (2006) Direct UV Raman Monitoring of 3_{10}- and π-Helix Premelting During α-helix unfolding, *J. Am. Chem. Soc.* (submitted for publication).
71. Manning, M. C., and Woody, R. W. (1991) Theoretical CD studies of polypeptide helices: Examination of important electronic and geometric factors, *Biopolymers 31*, 569−86.
72. Mikhonin, A. V., and Asher, S. A. (2005) Uncoupled Peptide Bond Vibrations in α-Helical and Polyproline II Conformations of Polyalanine Peptides, *J. Phys. Chem. B 109*, 3047−52.
73. Fodor, S. P., Copeland, R. A., Gryogon, C. A., and Spiro, T. G. (1989) Deep-ultraviolet Raman excitation profiles and vibronic scattering mechanisms of phenylalanine, tyrosine, and tryptophan, *J. Am. Chem. Soc. 111*, 5509−18.
74. Mikhonin, A. V., Bykov, S. V., Myshakina, N. S., and Asher, S. A. (2006) Peptide Secondary Structure Folding Reaction Coordinate: Correlation between UV Raman Amide III Frequency, ψ Ramachandran Angle, and Hydrogen Bonding, *J. Phys. Chem. B 110*, 5509−18.
75. Cartailler, J.-P., and Luecke, H. (2004) Structural and functional characterization of π bulges and other short intrahelical deformations, *Structure 12*, 133−44.
76. Higo, J., N., I., Kuroda, M., Ono, S., Nakajima, N., and Nakamura, H. K. (2001) Energy landscape of a peptide consisting of α-helix, 310-helix, β-turn, β-hairpin, and other disordered conformations, *Protein Sci. 10*, 1160−71.

BI060858M